Stray light characterization in a high-resolution imaging spectrometer designed for solar-induced fluorescence

Albert, Loren, Cushman, K. C., Allen, David, Zong, Yuqin, Alonso, Luis, et al.

Loren P. Albert, K. C. Cushman, David W. Allen, Yuqin Zong, Luis Alonso, James R. Kellner, "Stray light characterization in a high-resolution imaging spectrometer designed for solar-induced fluorescence," Proc. SPIE 10986, Algorithms, Technologies, and Applications for Multispectral and Hyperspectral Imagery XXV, 109860G (14 May 2019); doi: 10.1117/12.2519395

SPIE.

Event: SPIE Defense + Commercial Sensing, 2019, Baltimore, Maryland, United States

Stray light characterization in a high-resolution imaging spectrometer designed for solar-induced fluorescence

Loren P. Albert [a], K. C. Cushman [a,b], David W. Allen [c], Yuqin Zong [c], Luis Alonso [d], James R. Kellner *[a,b]

[a]Institute at Brown for Environment and Society, Brown University, Box 1951, 85 Waterman Street, Providence, RI 02912; [b]Department of Ecology and Evolutionary Biology, Brown University, Providence, RI 02912; [c]National Institute of Standards and Technology, Gaithersburg, MD 20899; [d]Image Processing Laboratory (IPL), University of Valencia, C/Catedrático José Beltrán, 2, Paterna, 46980 Valencia, Spain

ABSTRACT

New commercial-off-the-shelf imaging spectrometers promise the combination of high spatial and spectral resolution needed to retrieve solar induced fluorescence (SIF). Imaging at multiple wavelengths for individual plants and even individual leaves from low-altitude airborne or ground-based platforms has applications in agriculture and carbon-cycle science. Data from these instruments could provide insight into the status of the photosynthetic apparatus at scales of space and time not observable with tools based on gas exchange, and could support the calibration and validation activities of current and forthcoming space missions to quantify SIF. High-spectral resolution enables SIF retrieval from regions of strong telluric absorption by molecular oxygen, and also within numerous solar Fraunhofer lines in atmospheric windows not obscured by oxygen or water absorptions. Because the SIF signal can be < 5 % of background reflectance, rigorous instrument characterization and reduction of systematic error is necessary. Here we develop a spectral stray-light correction algorithm for a commercial off-the-shelf imaging spectrometer designed to quantify SIF. We use measurements from an optical parametric oscillator laser at 44 wavelengths to generate the spectral line-spread function and develop a spectral stray-light correction matrix using a novel exposure-bracketing method. The magnitude of spectral stray light in this instrument is small, but spectral stray light is detectable at all measured wavelengths. Examination of corrected line-spread functions indicates that the correction algorithm reduced spectral stray-light by 1 to 2 orders of magnitude.

Keywords: Remote sensing, chlorophyll fluorescence, photosynthesis, vegetation, unmanned aerial vehicle (UAV)

1. INTRODUCTION

Understanding photosynthesis at multiple spatial and temporal scales is critical for predicting the flux of carbon from the atmosphere to the biosphere.[1,2] Carbon uptake from photosynthesis can be estimated at the leaf level with gas exchange methods,[3,4] and for ecosystems using the eddy covariance method,[5,6] but metrics of photosynthesis are challenging to estimate at the scale between leaves and ecosystems, or at scales larger than ecosystems.[7,8] Solar-induced fluorescence (SIF) is an emission of light originating from chlorophyll. SIF is correlated with gross primary productivity.[9-11,12] Imaging spectrometers designed for spatially resolved estimates of SIF have recently been developed. These instruments may be used from airborne platforms and could provide insight into the status of the photosynthetic apparatus at scales of space and time that are not easily observable with other methods, and can also support calibration and validation activities of current and forthcoming space missions that aim to quantify SIF globally (e.g. OCO-2, OCO-3, and FLEX).[13-15]

Estimating SIF requires separating the SIF emission from reflected light, a process called, SIF retrieval.[16-18] Radiance spectra useful for quantifying SIF thus require sufficiently high spectral resolution to resolve solar Fraunhofer lines[18,19] or the telluric oxygen absorptions.[17,20] Because SIF is a small signal, estimating SIF also requires measurements with a high signal to noise ratio (SNR). For example, consider that vegetation reflectance in the region of chlorophyll fluorescence (approximately 650 nm to 800 nm)[12,21] is approximately 10 % of incoming light[22], and SIF is generally 1 to 5 % of reflected

*James_R_Kellner@brown.edu; phone 401-863-5768

Algorithms, Technologies, and Applications for Multispectral and Hyperspectral Imagery XXV, edited by Miguel Velez-Reyes, David W. Messinger, Proc. of SPIE Vol. 10986, 109860G

radiation in the far-red region.[12,16] This indicates that SIF is about three orders of magnitude smaller than incoming radiation. Thus, sources of uncertainty must be characterized and reduced.

Stray light, the unwanted scattered light from the optical and mechanical elements of the instrument, is a source of error that introduces a systematic uncertainty (i.e., a type B uncertainty) in all gratings-based spectrometers.[23] Stray light occurs when light entering a spectrometer is projected on the incorrect position of the detector array, which can occur along the spatial and spectral axes of the detector.[24,25] Here we describe how we (1) characterized spectral stray light in a commercial off-the-shelf imaging spectrometer designed for measurement of solar-induced fluorescence, (2) developed a spectral stray-light correction matrix (SLC matrix) to reduce spectral stray light for this instrument, (3) validated the spectral stray-light correction, and (4) developed a wavelength calibration for this instrument.

2. DESCRIPTION OF THE IMAGING SPECTROMETER

The imaging spectrometer was built and designed by Headwall Photonics and measures light within the 670 nm to 780 nm region of the electromagnetic spectrum.[26] To reduce the contribution of stray light originating outside the 670 nm to 800 nm region, a Semrock bandpass filter was affixed to the 25 mm lens. This filter transmits > 90 % of light between 662.5 nm and 799.5 nm, and < 0.01 % outside this region (300 nm to 662.5 nm, and 799.5 nm to 1200 nm). The focal plane is a 5.5-megapixel scientific CMOS image sensor (2560 × 2160 pixels). The slit image is projected onto 1600 (spatial) × 2160 (spectral) pixels of the image sensor, resulting in a nominal spectral sampling interval of 0.051 nm. During sensor operation, the temperature of the focal plane is stabilized using a thermoelectric cooler.

3. STRAY LIGHT CHARACTERIZATION AND CORRECTION

3.1 Spectral stray light correction method

Assuming that spectral stray light at each pixel along the spatial axis is the same, the spectral stray light errors of an imaging spectrometer can be characterized and corrected using the method described in Zong et al. (2006).[23] In brief, the magnitude of spectral stray light can be characterized by measuring a monochromatic light source - a spectral line source that does not have any emission other than the spectral line itself.[20] The detector response to a monochromatic source as a function of spectral position is the instrument line-spread function (LSF). The LSF can be decomposed into two regions: the narrow peak region is called the in-band (IB) response, and the out-of-band (OOB) region is the remaining broadband region with signals arising from stray light and other effects.[23] The IB region and the OOB region of the LSF can then be used to derive the spectral stray-light signal distribution function (SDF). This SDF can be generated for each element in the array to construct a SDF matrix, which can be used to derive a spectral SLC matrix, which is unique for each instrument.[23] The SLC matrix can be applied to raw signal data from the instrument to correct spectral stray light under normal operation. Note that this method reduces spectral stray light, but stray light can also be generated along the spatial axis (called spatial stray light), which we do not consider here.

3.2 Optical facility and measurements

To quantify the line-spread function (LSF), we focused the imaging spectrometer on a 25 mm diameter, 30-degree engineered holographic diffuser at a distance of 2.5 m (Figure 1). With this setup, the field of view of the imaging spectrometer was underfilled (i.e., only a small part of the spatial axis of the detector array near the center was illuminated) and the aperture stop of the imaging lens was overfilled by the diffuser, which was uniformly illuminated by a fiber-coupled 1 kHz pulsed optical parametric oscillator (OPO) laser source at NIST. The laser bandwidth is 0.2 nm. This high-power tunable OPO laser was operated by a custom LabVIEW program that controls the wavelength and intensity. The output power was optimized to maximize the signal at 10 ms integration time (see below) without saturating the detector response within the IB region of the LSF. The imaging spectrometer's response to narrow-band radiant flux across the spectral range (670 nm to 780 nm) was measured at increments of 2.5 nm, for a total of 44 responses. These response measurements provide data for deriving the SLC matrix.[20] We also measured the wavelength of each laser line using a laser spectrum analyzer with a wavelength uncertainty of a few picometers. We used this measured wavelength to produce a wavelength calibration for the imaging spectrometer.

The signal in the OOB region was several orders of magnitude weaker than the signal in the IB region, making it difficult to resolve both signals precisely at a single integration time. If the integration time was optimized for the IB to fill at least 80% of the dynamic range (in concert with the available laser power for a given wavelength), then much of the small signal in the OOB region was indistinguishable from the noise (Figure 2A black line). If the integration time was increased

enough to resolve the shape of the low signal for the OOB region, the IB region was totally saturated (Figure 2A blue line). Thus, to resolve the shape of both the IB region and OOB region, we used measurements from two integration times. We then combined the independent measurements from the IB and OOB regions using exposure bracketing (see next section), which is similar to techniques used for enhancing dynamic range in digital photography. For each laser wavelength, measurements with 10 ms and 1000 ms integration times were collected in sequence. Dark measurements (with all lights off or covered) were made after every 5 laser-line measurements for each corresponding integration time. A test of dark measurement stability using these periodic dark measurements showed negligible changes over time; the mean of each dark-measurement collection was within 0.5 DN units, and the coefficient of determination (r^2) for a linear model with time as a factor was < 0.001. This indicates that the dark current is stable when measured in the laboratory under controlled temperatures.

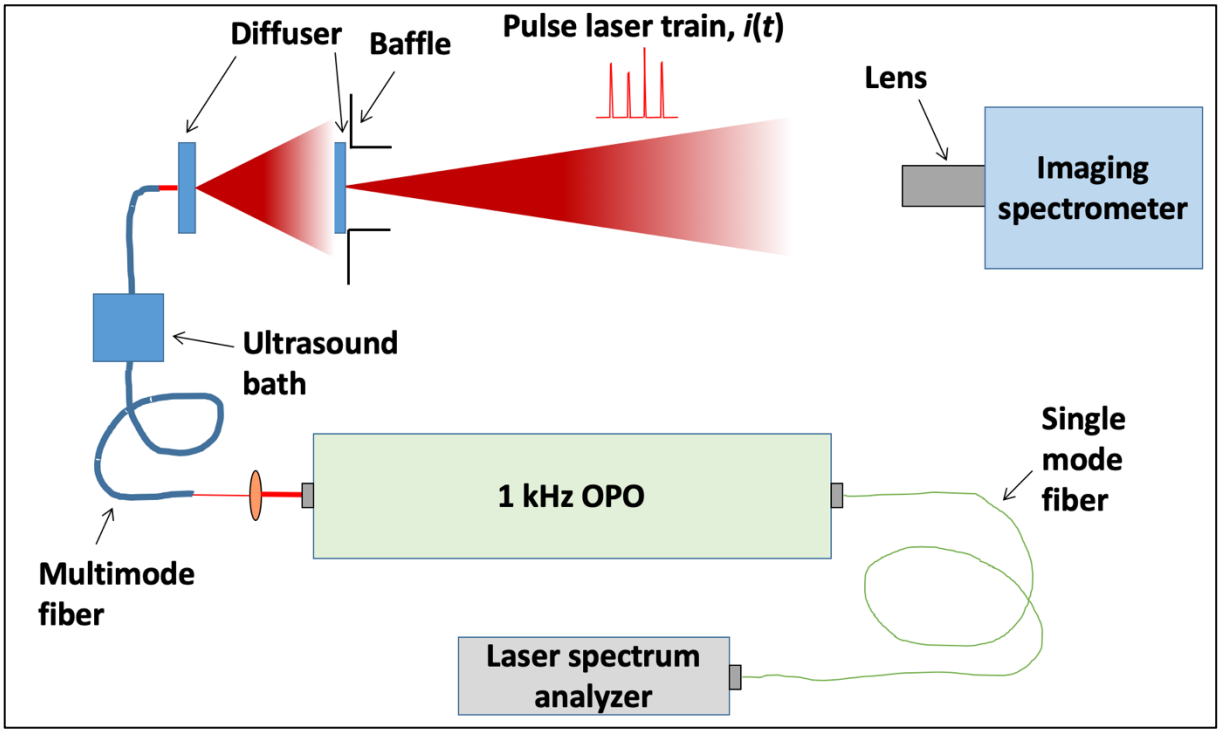

Figure 1. Schematic diagram of the set-up for making measurements of a monochromatic light source for development of the spectral stray-light correction matrix. The imaging spectrometer was illuminated with narrow-band radiant flux generated by a 1 kHz pulsed optical parametric oscillator (OPO) laser source. We tuned the OPO laser to quantify the line-spread function at 44 wavelengths in increments of 2.5 nm across the spectral range of the imaging spectrometer.

3.3 Developing the SLC matrix

For each laser line measurement, we computed the spectral line-spread function at spectral pixel λ recorded at integration time t according to the equation:

$$LSF_{\lambda,t} = \frac{(\frac{1}{n}\sum_{i=1}^{n} DN_{\lambda,t,signal} - \frac{1}{n}\sum_{i=1}^{n} DN_{\lambda,t,dark})}{t}$$

Here, $LSF_{\lambda,t}$ is the dark-subtracted mean response in digital number (DN) units divided by the integration time, t, in milliseconds. The line-spread function over all spectral pixels for a given integration time is denoted LSF_t. We combined LSF_{10} and $LSF_{1,000}$ into a single LSF response for each recorded laser line using exposure bracketing. Exposure bracketing was necessary because measurements at the long integration time saturated the detector response in the IB region, and measurements at the short integration time did not resolve stray light in the OOB region. Combining measurements from two integration times resolved the LSF. Exposure bracketing required aligning the two line-spread functions along the scaled DN axis. This was necessary because $LSF_{\lambda,t}$ can be sensitive to small fluctuations in laser power. To remove the impact of these fluctuations, we determined a multiplicative correction factor (b_1) by fitting the following linear model:

$$LSF_{\lambda,1,000} = b_0 + b_1 \times LSF_{\lambda,10}$$

We assumed that $b_0 = 0$. We fit the model using data within windows that were 40 spectral pixels wide. The positions of these windows were selected to avoid the region of saturation present in the 1,000 ms integration time measurements. They also avoided the region where the 10 ms integration time measurements did not rise above the noise threshold. After applying the multiplicative correction factor to $LSF_{\lambda,10}$ we spliced the corrected $LSF_{\lambda,10}$ with $LSF_{\lambda,1,000}$ to produce LSF_{λ}. Following Zong et al. (2006)[23], we generated the stray-light distribution function (SDF) by normalizing LSF_{λ} to the total IB area and setting values in the IB region equal to zero. After generating the SDF for each of the 44 LSF_{λ}, we used linear interpolation to produce a SDF matrix for all 2,160 spectral pixels. We emphasize that the SDF matrix developed here is from measurements at a single position along the spatial axis of the detector, and we therefore assume that SDF is invariant with respect to the spatial axis.

3.4 Validation of the SLC matrix

We applied the spectral SLC matrix to the laser line dataset to examine the effect of SLC correction on the OOB signal. We also applied the spectral SLC matrix to independent light sources and filters with known spectral properties (validation sources). With the imaging spectrometer, we measured 100 frames of the following sources at NIST: a 700 nm longpass filter (Omega Optical, 3RD millennium) for 150 ms, and an LED light source with a peak at 700 nm (Thorlabs LED model M700L4) for 500 ms. The optical filter was attached to the first diffuser and was illuminated by a quartz tungsten halogen lamp-based fiber illuminator with a collimated beam. The collimated output of the fiber illuminator and the LED were placed at the same position as the fiber of the OPO laser. To apply the SLC correction to the laser line dataset and the validation source dataset, a single matrix multiplication operation was performed using the dark-subtracted mean response following Zong et al (2006)[23].

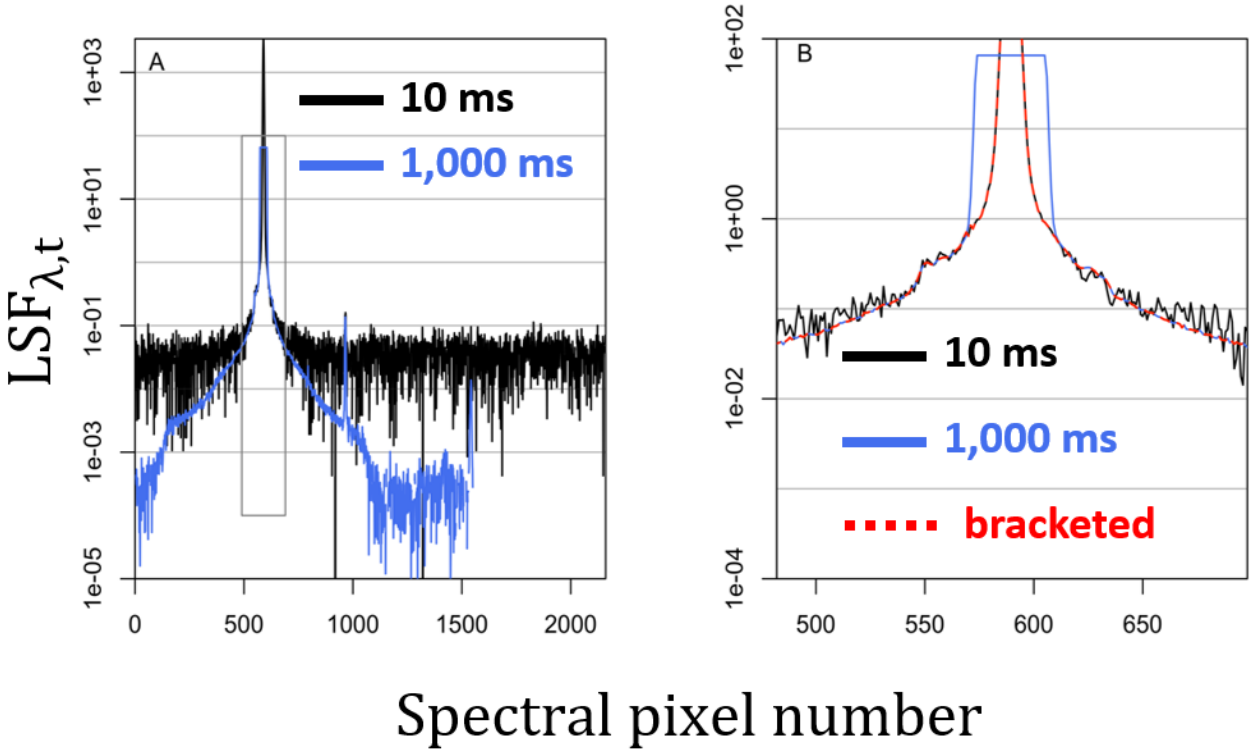

Figure 2. Demonstration of exposure bracketing to obtain a well-resolved line-spread function (LSF_{λ}). (A) We quantified the LSF at integration times of 10 ms and 1000 ms. (B) We used exposure bracketing to combine data from the two integration times (inset from panel A). $LSF_{\lambda,1,000}$ (blue) is overlaid on $b_1 \times LSF_{\lambda,10}$ (black). The exposure-bracketed estimate that combines data from two integration times is the dotted red line.

3.5 Instrument wavelength calibration

We quantified the relationship between wavelength (nm) and spectral pixel number using the spectral lines produced by the OPO laser at NIST.[26] The spectral pixel number of the peak response for each laser line was associated with the measured wavelength of the OPO laser for each laser line. We used ordinary linear regression to develop an equation that predicts wavelength as a function of spectral pixel number, and we used this equation to determine the wavelength of each of the 2,160 spectral pixels on the focal plane. (We excluded the laser line at 710 nm from the regression analysis because the laser power at 710 nm is too low for the laser spectrum analyzer to measure the wavelength.)

4. RESULTS

4.1 Spectral stray light characterization and correction results

Spectral stray light was detectable for all 44 laser lines across the spectral axis of the focal plane, with no apparent trend in the magnitude of spectral stray light across the spectral axis of the detector. Application of the spectral SLC matrix to the laser line measurements showed that the spectral SLC matrix reduced spectral stray light by approximately one order of magnitude close to the IB region where spectral stray light was greatest (Figure 3). Application of the spectral SLC matrix also reduced the stray light signal in the OOB region far from the laser line (greater than 400 spectral pixels, or about 20 nm, away from the laser line; Figure 3).

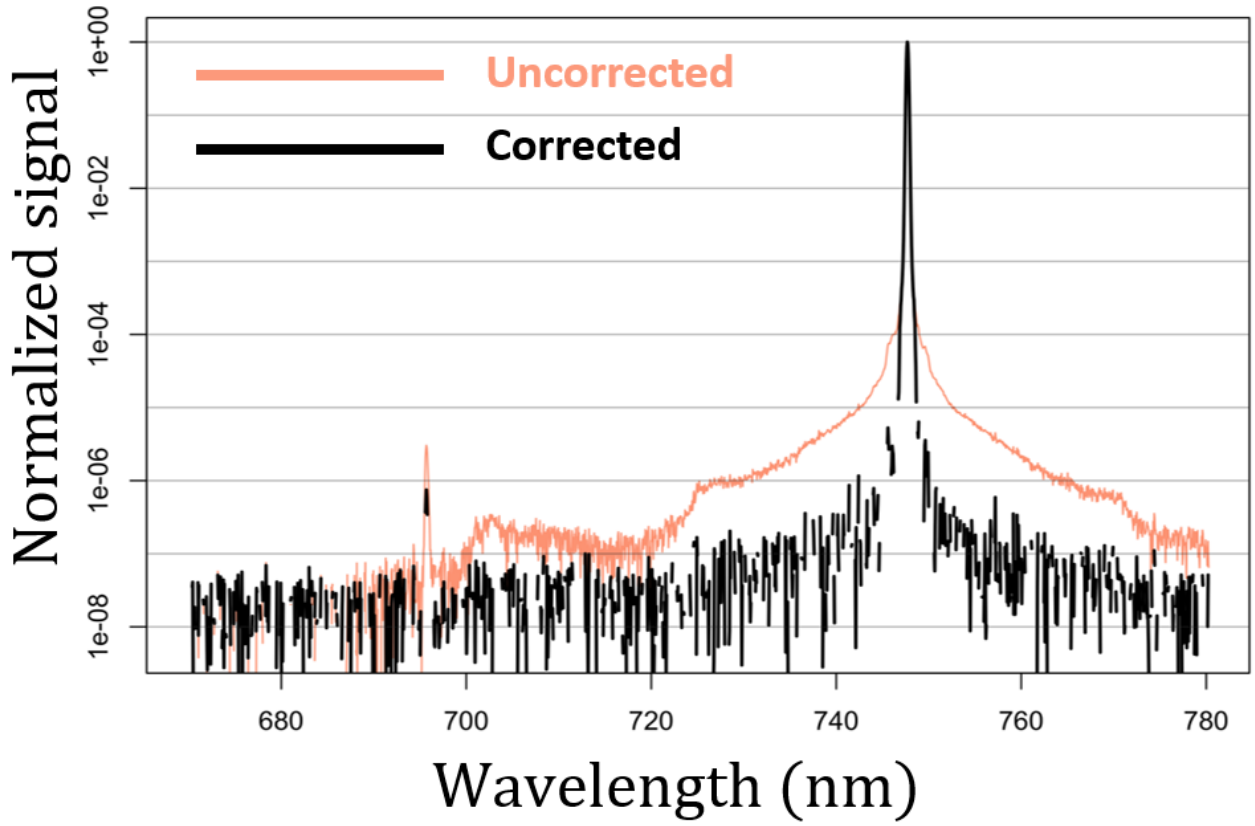

Figure 3. Example $LSF_{\lambda,1,000}$ from a monochromatic laser source before (orange line) and after (black line) applying a stray-light correction. The function is normalized to the peak signal for visualization. Some values were negative after the dark-noise subtraction. Negative values are undefined on the log scale.

Examination of validation sources indicates that the spectral SLC matrix effectively reduces spectral stray light (Figure 4A). However, the contribution of stray light to the measurement of Source A is low in comparison to a typical high-end spectrometer,[23] so the effect of the correction is small. The small stray light signal of our instrument is caused by the

narrow spectral range of the instrument (110 nm), and a bandpass optical filter on the lens that blocks radiation outside the spectral range of the imaging spectrometer (Figure 4A). Stray light in the measurement of Source B is much less apparent because of the LED source spectrum (Figure 4B).

4.2 Wavelength calibration results

The relationship between wavelength (nm) and spectral pixel number using 43 spectral lines produced by the OPO laser at NIST indicated a strong linear relationship (Figure 5). The intercept was 669.819 nm ($\pm$ 1.02 $\cdot$ 10^{-2} SE), and the slope of the relationship was 0.0511 ($\pm$ 8.05 $\cdot$ 10^{-6} SE) nm $\cdot$ pixel^{-1}. The coefficient of determination (r^2) was > 0.999.

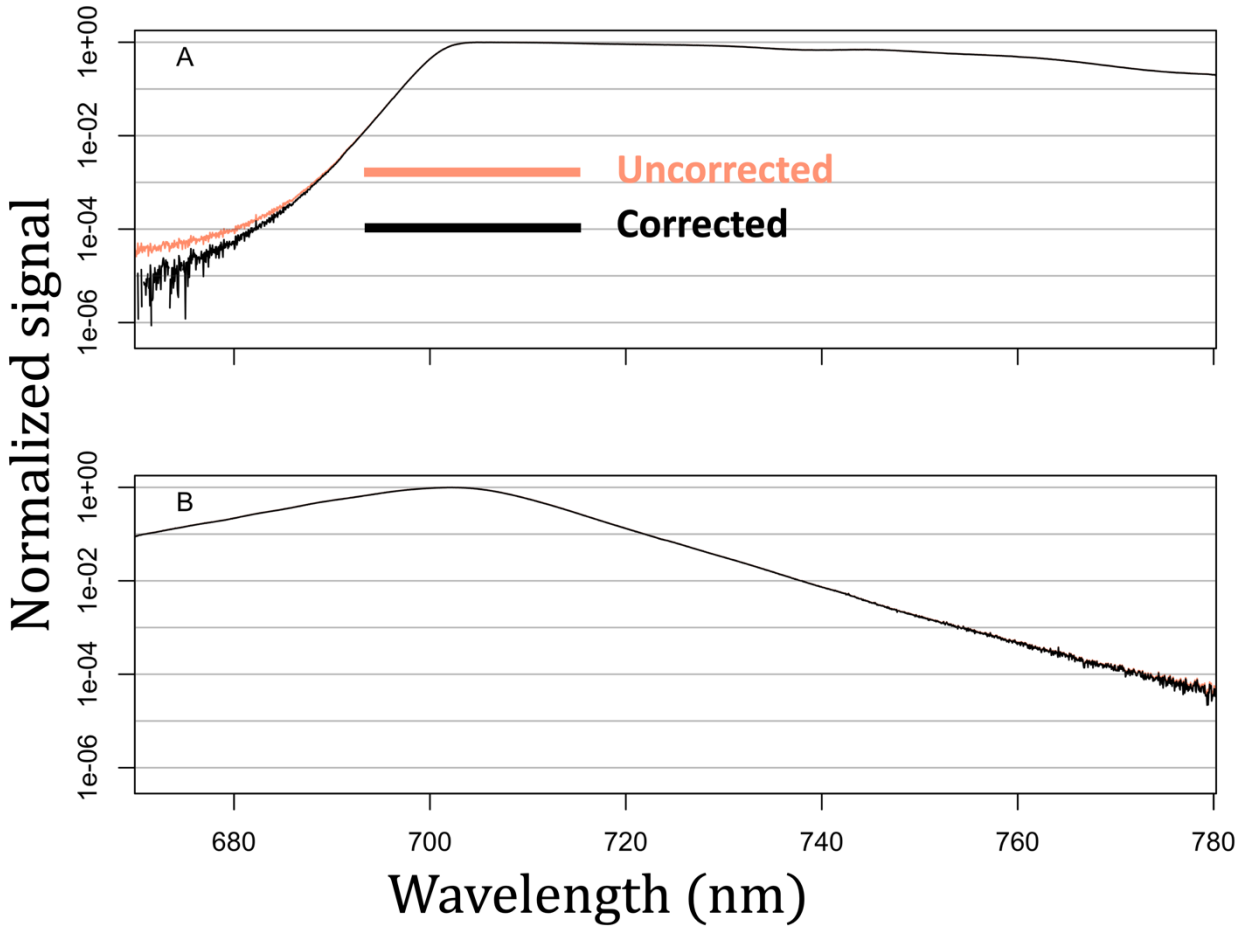

Figure 4. Measured light from validation light sources before (orange line) and after (black line) applying a stray-light correction. To evaluate the stray-light correction procedure, we measured a validation filter in the presence of a quartz tungsten halogen lamp fiber illuminator with a collimated beam. (A) 700 nm longpass filter (Omega Optical, 3RD millennium). (B) an LED light source with a peak at 700 nm. Each signal was normalized to the peak signal for visualization.

5. CONCLUSIONS

Solar-induced fluorescence has the potential to become a transformative measurement in studies of photosynthesis and gross primary productivity at multiple scales,[7,27,28] and imaging of solar-induced fluorescence may reveal fine-scale heterogeneity in plant stress or productivity.[29] However, SIF is a small signal, and can only be detected by instruments with high spectral resolution and measurements with high SNR. Stray light is one source of systematic error that can be characterized and reduced.[23] Although the spectral stray light signal for the imaging spectrometer we examined was small,

it remains a significant consideration in comparison to the small SIF signal, which is generally 1 – 5% of reflectance in the far-red region region.[12,16]

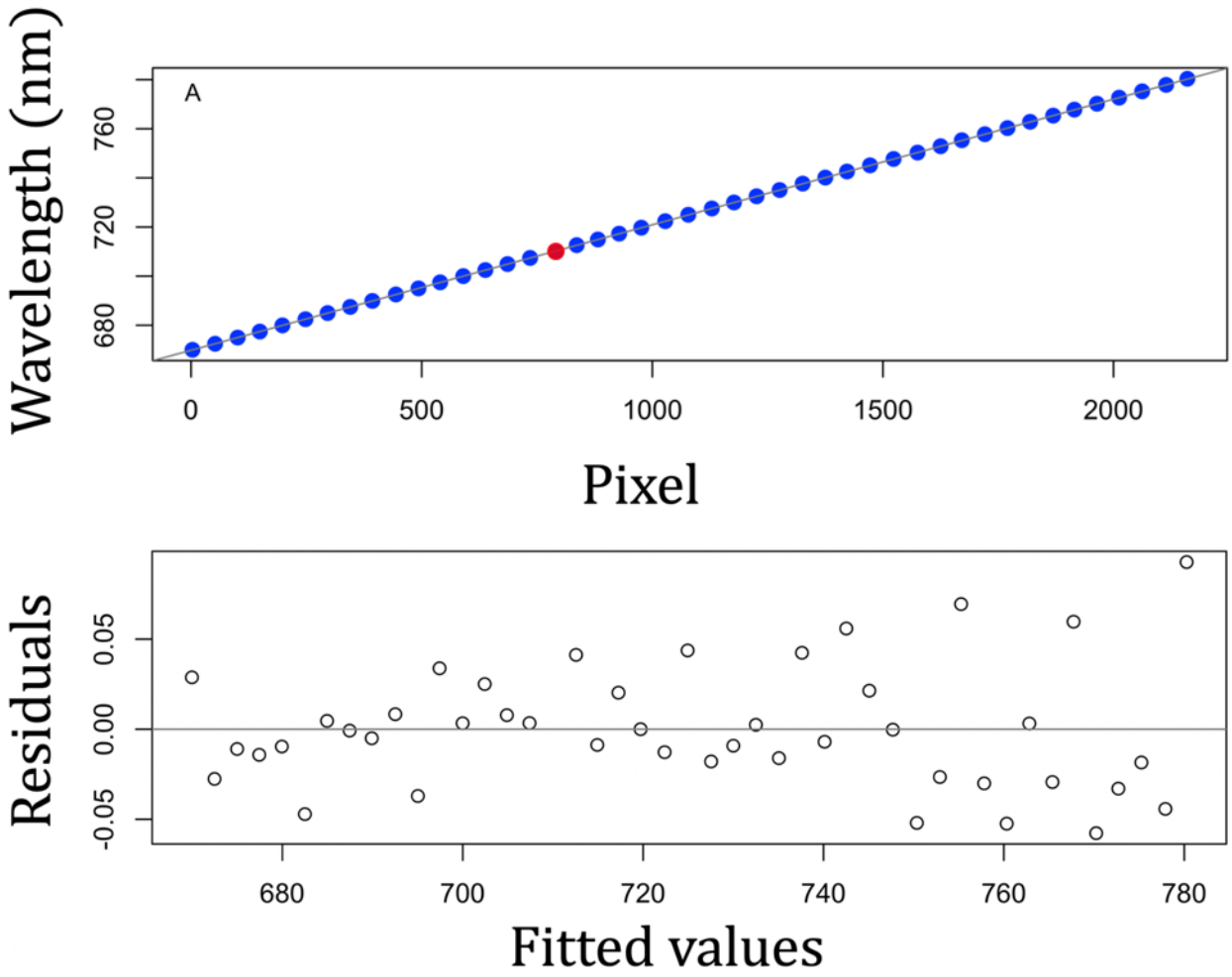

Figure 5. Wavelength calibration for a high-resolution imaging spectrometer designed to quantify solar induced fluorescence. A tunable laser source was aimed directly at the spectrometer then tuned to 44 positions throughout the 670 nm – 780 nm region. We regressed the measured wavelengths on the spectral pixel that was associated with the maximum DN response to laser emission. We excluded the laser measurement at 710 nm (red dot in panel A) from the regression analysis because the laser power at 710 nm was too low for the laser spectrum analyzer to measure the wavelength. The slope of an ordinary least squares regression line is 0.0511 nm · pixel^{-1} and the intercept 669.819 nm (panel A). The maximum absolute residual was 0.093 nm (panel B).

Because stray light calibrations are instrument-specific, future users of commercial off-the-shelf imaging spectrometers designed for SIF estimation will need to characterize and reduce spectral stray light in their particular instrument(s). One lesson from this study is that exposure-bracketing the LSF from two integration times can help resolve the IB region and the OOB region. Another option may be to use a small integration time that resolves the peak signal while averaging many frames to resolve the OOB response. Here we used 100 frames, and we found that the stray light in the OOB region remained indistinguishable from the noise with 10 ms to 100 ms integration times. It would be informative to test whether the mean of 1000 frames of 100 ms integrations enables resolution of spectral stray light in the OOB region.

One method of estimating SIF by separating SIF from vegetation reflectance depends upon resolution of Fraunhofer lines[18,19] Fraunhofer lines are narrow, and resolving Fraunhofer lines thus requires high spectral resolution. Here we characterized the spectral sampling interval based on the detector response to an OPO laser emission, Wavelength

calibration shows that spectral sampling interval is 0.0511 nm · $pixel^{-1}$, which is consistent with manufacturer specifications.

Future work will include characterizing other possible sources of error for this instrument, including detector nonlinearity and spatial stray light.[24,25,30] Point spread measurements can be used to characterize spatial stray light, and future work in imaging spectroscopy of solar-induced fluorescence should quantify the contribution of spatial stray light. Robust instrument characterization and calibration of imaging spectrometers used to estimate SIF at high spatial resolution could support the calibration and validation activities of current and forthcoming space missions to quantify SIF globally (OCO-2, OCO-3, and FLEX).

ACKNOWLEDGEMENTS

Loren Albert is supported by a Voss postdoctoral fellowship at the Institute at Brown for Environment and Society. This research was supported by grants from the Institute at Brown for Environment and Society at Brown University. Luis Alonso is partially funded by AVANFLEX project (Advanced Products for the FLEX mission), n° ESP2016-79503-C2-1-P, Ministry of Economy and Competitiveness, Spain.

REFERENCES

[1] Schimel, D., Pavlick, R., Fisher, J. B., Asner, G. P., Saatchi, S., Townsend, P., Miller, C., Frankenberg, C., Hibbard, K., et al., "Observing terrestrial ecosystems and the carbon cycle from space," 1762–1776 (2015).

[2] Friedlingstein, P., Meinshausen, M., Arora, V. K., Jones, C. D., Anav, A., Liddicoat, S. K., Knutti, R., "Uncertainties in CMIP5 Climate Projections due to Carbon Cycle Feedbacks," J. Climate **27**(2), 511–526 (2014).

[3] Flexas, J., Escalona, J. M., Evain, S., Gulias, J., Moya, I., Osmond, C. B., Medrano, H., "Steady-state chlorophyll fluorescence (F_S) measurements as a tool to follow variations of net CO_2 assimilation and stomatal conductance during water-stress in C_3 plants," Physiol Plant **114**(2), 231–240, Wiley/Blackwell (10.1111) (2002).

[4] Long, S. P., Bernacchi, C. J., "Gas exchange measurements, what can they tell us about the underlying limitations to photosynthesis? Procedures and sources of error," Jo. Exp. Bot. **54**(392), 2393–2401 (2003).

[5] Burba, G., Eddy Covariance Method, LI-COR Biosciences (2013).

[6] Baldocchi, D., "Measuring fluxes of trace gases and energy between ecosystems and the atmosphere - the state and future of the eddy covariance method," Glob. Change Biol. **20**(12), 3600–3609 (2014).

[7] Porcar-Castell, A., Tyystjarvi, E., Atherton, J., van der Tol, C., Flexas, J., Pfundel, E. E., Moreno, J., Frankenberg, C., Berry, J. A., "Linking chlorophyll a fluorescence to photosynthesis for remote sensing applications: mechanisms and challenges," Jo. Exp. Bot. **65**(15), 4065–4095 (2014).

[8] Rascher, U., Alonso, L., Burkart, A., Cilia, C., Cogliati, S., Colombo, R., Damm, A., Drusch, M., Guanter, L., et al., "Sun-induced fluorescence - a new probe of photosynthesis: First maps from the imaging spectrometer HyPlant," Glob. Change Biol. **21**(12), 4673–4684 (2015).

[9] Guanter, L., Zhang, Y., Jung, M., Joiner, J., Voigt, M., Berry, J. A., Frankenberg, C., Huete, A. R., Zarco-Tejada, P., et al., "Global and time-resolved monitoring of crop photosynthesis with chlorophyll fluorescence," Proceedings of the National Academy of Sciences **111**(14), E1327–E1333 (2014).

[10] Xiao, J., Li, X., He, B., Arain, M. A., Beringer, J., Desai, A. R., Emmel, C., Hollinger, D. Y., Krasnova, A., et al., "Solar-induced chlorophyll fluorescence exhibits a universal relationship with gross primary productivity across a wide variety of biomes," Glob. Change Biol. **25**(4), e4–e6 (2019).

[11] Li, X., Xiao, J., He, B., Altaf Arain, M., Beringer, J., Desai, A. R., Emmel, C., Hollinger, D. Y., Krasnova, A., et al., "Solar-induced chlorophyll fluorescence is strongly correlated with terrestrial photosynthesis for a wide variety of biomes: First global analysis based on OCO-2 and flux tower observations," Glob. Change Biol. **24**(9), 3990–4008 (2018).

[12] Frankenberg, C., Berry, J., 3.10 Solar Induced Chlorophyll Fluorescence: Origins, Relation to Photosynthesis and Retrieval, Comprehensive Remote Sensing, 143–162, Elsevier (2017).

[13] Drusch, M., Moreno, J., Del Bello, U., Franco, R., Goulas, Y., Huth, A., Kraft, S., Middleton, E. M., Miglietta, F., et al., "The FLuorescence EXplorer Mission Concept—ESA's Earth Explorer 8," IEEE Trans. Geosci. Remote Sensing **55**(3), 1273–1284 (2016).
[14] Stavros, E. N., Schimel, D., Pavlick, R., Serbin, S., Swann, A., Duncanson, L., Fisher, J. B., Fassnacht, F., Ustin, S., et al., "ISS observations offer insights into plant function," Nat. ecol. evol. **1**(7), 8830–8835 (2017).
[15] Sun, Y., Frankenberg, C., Wood, J. D., Schimel, D. S., Jung, M., Guanter, L., Drewry, D. T., Verma, M., Porcar-Castell, A., et al., "OCO-2 advances photosynthesis observation from space via solar-induced chlorophyll fluorescence," Science **358**(6360), eaam5747, American Association for the Advancement of Science (2017).
[16] Meroni, M., Rossini, M., Guanter, L., Alonso, L., Rascher, U., Colombo, R., Moreno, J., "Remote sensing of solar-induced chlorophyll fluorescence: Review of methods and applications," Remote Sens. Environ. **113**(10), 2037–2051, Elsevier Inc. (2009).
[17] Joiner, J., Yoshida, Y., Vasilkov, A. P., Corp, L. A., Middleton, E. M., "First observations of global and seasonal terrestrial chlorophyll fluorescence from space," 637–651 (2011).
[18] Plascyk, J. A., "The MK II Fraunhofer Line Discriminator (FLD-II) for Airborne and Orbital Remote Sensing of Solar-Stimulated Luminescence," OPEGAR **14**(4), 144339, International Society for Optics and Photonics (1975).
[19] Frankenberg, C., Butz, A., Toon, G. C., "Disentangling chlorophyll fluorescence from atmospheric scattering effects in O 2A-band spectra of reflected sun-light," Geophysical Res. Lett. **38**(3), L03801, Wiley-Blackwell (2011).
[20] Moya, I., Camenen, L., Latouche, G., Mauxion, C., Evain, S., Cerovic, Z. G., "An Instrument for the Measurement of Sunlight Excited Plant Fluorescence," [Photosynthesis: Mechanisms and Effects], Springer Netherlands, Dordrecht, 4265–4270 (1998).
[21] Franck, F., Juneau, P., Popovic, R., "Resolution of the Photosystem I and Photosystem II contributions to chlorophyll fluorescence of intact leaves at room temperature.," Biochim. Biophys. Acta **1556**(2-3), 239–246 (2002).
[22] Asner, G. P., Heidebrecht, K. B., "Spectral unmixing of vegetation, soil and dry carbon cover in arid regions: Comparing multispectral and hyperspectral observations," International Journal of Remote Sensing **23**(19), 3939–3958 (2010).
[23] Zong, Y. Q., Brown, S. W., Johnson, B. C., Lykke, K. R., Ohno, Y., "Simple spectral stray light correction method for array spectroradiometers," Appl Opt **45**(6), 1111–1119 (2006).
[24] Zong Y., Brown S. W., Lykke K. R., and Ohno Y., "Correction of stray light in spectroradiometers and imaging instruments," Proc. CIE, July 4-11, 2007, Beijing, China, CIE 178:2007, D2-33 to D2-36.
[25] Zong, Y., Brown, S. W., Meister, G., Barnes, R. A., Lykke, K. R., "Characterization and correction of stray light in optical instruments," Proc. of SPIE, September 17-20, 2007, Florence, Italy, Vol. 6744, 67441L-1-11.
[26] "Note: References are made to certain commercially available products in this paper to adequately specify the experimental procedures involved. Such identification does not imply recommendation or endorsement by the National Institute of Standards and Technology, nor does it imply that these products are the best for the purpose specified."
[27] Gu, L., Wood, J. D., Chang, C. Y. Y., Sun, Y., Riggs, J. S., "Advancing Terrestrial Ecosystem Science With a Novel Automated Measurement System for Sun-Induced Chlorophyll Fluorescence for Integration With Eddy Covariance Flux Networks," J. Geophys. Res. Biogeosci. **124**(1), 127–146 (2019).
[28] Moya, I., Flexas, J., "Remote sensing of photosynthesis," [*Terrestrial Photosynthesis in a Changing Environment: A Molecular, Physiological and Ecological Approach*], Cambridge university Press, 1–18 (2012).
[29] Rascher, U., Alonso, L., Burkart, A., Cilia, C., Cogliati, S., Colombo, R., Damm, A., Drusch, M., Guanter, L., et al., "Sun-induced fluorescence - a new probe of photosynthesis: First maps from the imaging spectrometer HyPlant," Glob. Change Biol. **21**(12), 4673–4684 (2015).
[30] Grossmann, K., Frankenberg, C., Magney, T. S., Hurlock, S. C., Seibt, U., Stutz, J., "PhotoSpec: A new instrument to measure spatially distributed red and far-red Solar-Induced Chlorophyll Fluorescence," 311–327 (2018).